

Supporting Information

Manipulating anion solvation competitiveness via a multifunctional additive toward robust low-temperature sodium metal batteries

Tonghui Zhang,^a Ying Xiao,^{*a} Shunshun Zhao,^a Yu Han,^a Gang He,^a Shimou Chen ^{*a}

State Key Laboratory of Chemical Resource Engineering, Beijing Key Laboratory of Electrochemical Process and Technology of Materials, National Engineering Research Center for Fuel Cell and Hydrogen Source Technology, Beijing University of Chemical Technology, Beijing 100029, P. R. China

E-mail: yxiao@buct.edu.cn; chensm@buct.edu.cn

Experimental section

Materials.

Diethylene glycol dimethyl ether (DG) (>99.0 %, GC) and sodium hexafluorophosphate (NaPF₆) were received from Aladdin, pentafluoro(phenoxy)cyclotriphosphazene (FPPN) was ordered from Beijing Huawei Ruike Chemical Technology Co., Ltd. The Na₃V₂(PO₄)₃ cathode material and HC were purchased from Dongguan Kerude Experimental Equipment Technology Co., Ltd,

Electrolytes.

0.5M-D: 0.5M NaPF₆ in DG

0.5M-FD: 0.5M NaPF₆ in DG with 0.20 wt.% FPPN

Battery cell fabrication

Electrochemical tests were conducted using CR-2025-type coin cells. The electrode material and polyvinylidene fluoride (PVDF, MTI Co., Ltd.) were mixed in the N-methyl pyrrolidinone (NMP, Sigma Aldrich) solvent at a mass ratio of 8:1:1 using a weighing bottle and homogenized by overnight magnetic stirring. The resulting slurry was then spread onto a carbon-coated aluminum foil (Al/C) using a doctor's blade. The obtained cathode film was dried at 80 °C for 1 hour in a blast oven and subsequently for 12 hours at 80 °C in a vacuum oven. For coin cell assembly, the cathode was prepared by punching discs (12 mm in diameter), and the typical mass loading of Na₃V₂(PO₄)₃ active material is 1- 2 mg cm⁻². For pouch cell assembly, the cathode was prepared by cutting into 3 × 4 cm rectangles, with a mass loading of 1.4 mg cm⁻². The separator consists of a Whatman glass fiber sandwiched between two Celgard 2325 films. Na||Al cells were fabricated by pairing a Na metal foil (φ 14 mm) with an Al/C foil (φ 16 mm), Na||Na symmetric cells were assembled using Na metal foils (φ 12 mm and φ 14 mm), and Na||NVP half cells were assembled with a Na metal foil (φ 14 mm) and a prepared NVP cathode (φ 12 mm). Pouch cells were assembled by NVP cathode films (3 cm × 4 cm) with Na metal anode, then packaged by Al-plastic films.

Electrochemical measurements

The cycling performance, rate capability of cells, and the charge-discharge test were all performed on a standard battery tester (CT4008, Neware). The cycling performance of Na||NVP half cells was obtained at 0.3 C and 1 C (1 C = 117 mA g⁻¹). For conventional Na||Na symmetric cell cycling tests, 0.1, 0.5, and 1.0 mAh cm⁻² of Na was repeatedly stripped/plated with the current density of 0.1, 0.5, and 1.0 mA cm⁻², respectively. EIS tests of Na||Na and Na||NVP cells were carried out using an electrochemical workstation (Autolab PGSTAT302N, Netherlands) with a 10 mV perturbation in the frequency range of 0.01 Hz to 1×10⁵ Hz.

The ionic conductivities of electrolytes were measured by assembling symmetric stainless-steel cells. The electrolytic conductivity value was obtained from the impedance spectroscopy by the following

equation:

$$\sigma = \frac{L}{R_b S} \quad (1)$$

where R_b is the ohmic resistance, S is the area, and L is the space between two stainless steel electrodes, respectively. The data points from 25 °C to -40 °C were measured by an AUTOLAB electrochemical station (NOVA) in the frequency range of 0.01 Hz to 1×10^5 Hz. The activation energy was calculated based on the following Arrhenius equation⁵¹⁻⁵³:

$$\sigma = A \exp\left(-\frac{E_a}{k_B T}\right) \quad (2)$$

Where A is a pre-exponential factor, k_B is the Boltzmann constant, E_a is the activation energy and T is the absolute temperature.

The Na^+ transference numbers of electrolytes were determined by the potentiostatic polarization technique using an AUTOLAB electrochemical station (NOVA). A voltage of 5 mV was applied to a $\text{Na}||\text{Na}$ cell for 2 h to measure the initial current I_0 , which is derived from both cation and anion transfer in the electrolyte. The steady-state current I_{SS} is solely attributed to the transportation of Na^+ ions. Electrochemical impedance spectroscopy (EIS) measurements were conducted before and after the polarization step to obtain the impedance of the cells. The transference number was calculated by the following equation:

$$t_{\text{Na}^+} = \frac{I_{SS}(\Delta V) I_0 R_0}{I_0(\Delta V) I_{SS} R_{SS}} \quad (3)$$

where ΔV is the applied bias voltage, R_0 is the initial impedance, and R_{SS} is the steady-state impedance, I_0 is the initial current, and I_{SS} is the steady-state current.

Physical Characterization

Scanning electron microscope (SEM) images were obtained on S4700 (Hitachi) with the accelerating voltage of 5 kV. Transmission electron microscope (TEM) analysis was performed on JEM 3010 (JEOL) with the accelerating voltage of 300 kV. The nuclear magnetic resonance (NMR) spectrum was obtained on AV600 (Bruker 600MHz). Raman spectra of the electrolytes were recorded with the LabRAM HR Evolution instrument (Horiba) with excitation line of 532 nm. The electrolytes are loaded in transparent quartz cuvette, and then collected with 50 and 100× objective lens and 50% laser power for 10 seconds. X-ray photoelectron spectroscopy (XPS) conducted on Nexsa (Thermo Kalpha) with a monochromatic Al K α X-ray source (excitation energy = 1486.6 eV) was used and the binding energy values of all the data were referenced to the C 1s peak (284.8 eV), accompanied with depth profiling which was obtained by Ar^+ sputtering at 1 kV for 0, 60, 120, 180 s.

The specimens of XPS were the NVP cathodes and Na anodes in Na||NVP cells after 50 cycles at 1 C and in Na||Na cells at 1 mA cm⁻². The samples for TEM were NVP cathodes in Na||NVP cells after 50 cycles at 1 C. The test samples for SEM in Na||Al cells at 0.5 mA cm⁻².

The tested data in this article are mainly accurate to two decimal places.

Computational details

Molecular Dynamics (MD) simulations of these two sodium ion electrolyte systems were carried out using the Gromacs program suite with the hybridized force field of CL&P forcefield and OPLS-AA force field.⁵⁴ The sodium cation was parameterized using the CL&P force field, and a charge scaling of 0.65 was adopted to mimic polarization and charge transfer effects. Other organic molecules were simulated using OPLS-AA forcefield. All these topology files of these molecules and ions were generated directly using the all-atom and ionic-liquid modules of the AuToFF web server.

The initial simulation boxes contained the electrolyte components, with dimensions of 10×10×10 nm³, were created using the packmol program, and the mole ratios of each component were quintuple as our experiments. The structures were first energy-minimized and then annealed from 0 to 400 K and then cooled down over a 1 ns time period with a time step of 1 ps to reach an equilibrium state. The temperature was maintained at 298.15 K using the velocity-rescale thermostat with a relaxation constant of 1 ps. The pressure was maintained at 1.01325×10⁵ Pa using Berendsen's barostat with an isothermal compressibility constant of 4.5×10⁻⁵. Periodic boundary conditions were applied in all directions, and the electrostatic interactions and van der Waals forces were treated using the Particle-mesh Ewald (PME) method with a cut-off distance of 15 Å.

Following the energy minimization and equilibration steps, a 20 ns MD simulation at NVT ensemble was performed, with the trajectory saved every 1 ps. The further statistics results including the radial distribution function (RDF) and solvation structures, were all analyzed from the trajectory data by Gromacs tool-suites. The simulation box was rendered using the Visual Molecular Dynamic program (VMD).

The Binding energy and ESP were calculated with the Gaussian 16 software.⁵⁵ The B3LYP functional was adopted for all calculations in combination with the D3BJ dispersion correction. For geometry optimization and frequency calculations, a 6-31G (d, p) basis set was used for all atoms. Electrostatic potential analyses are performed in Multiwfn and VMD packages.

The finite element simulation was carried out using COMSOL Multiphysics 6.2, and the ion flux field was simulated using the "cubic current distribution" physical field. Ion concentration follows Fick's first law of diffusion, while electromigration follows the Nernst-Planck relationship. Both models take into account the structure of the simplified research space. The lengths of the two electrodes are 10 μm and the distance between them is 5.5 μm. The main body of the simulation solution is the electrode-electrolyte interface. The boundary conditions are set with the positive electrode as the zero potential boundary and the negative electrode potential as the polarization voltage of the battery. The initial sodium ion concentration is set at 0.5M. The diffusion coefficients of Na⁺ in the electrolyte were set to 4×10⁻¹⁴ m²/s and 6×10⁻¹⁴ m²/s respectively. The exchange current density through the battery is set to 1 mA cm⁻². The system temperature is set at 298 K.

Figures

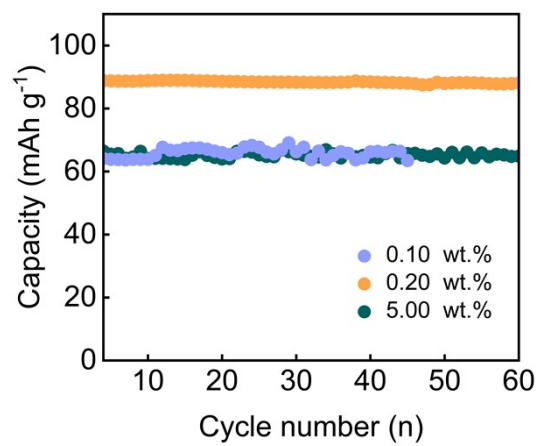


Fig. S1 The electrochemical performance of Na||NVP cells using electrolytes with different FPPN contents tested at 1 C and -20 °C.

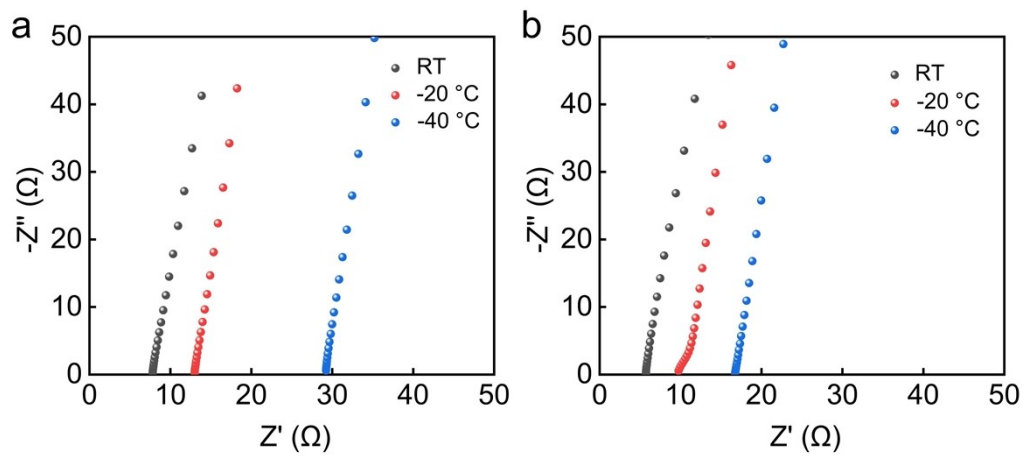
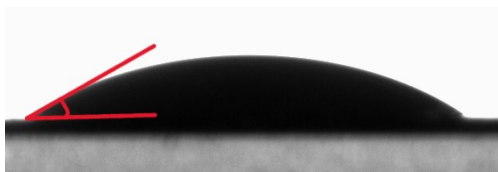


Fig. S2 Electrochemical impedance spectra of the steel||steel symmetric cells with (a) 0.5M-D electrolyte, (b) 0.5M-FD electrolyte at different temperatures.

0.5M-D
Contact angel: 31.40°



0.5M-FD
Contact angel: 31.10°



Fig. S3 Wettability test of the 0.5M-D and 0.5M-FD electrolytes on bare Na.

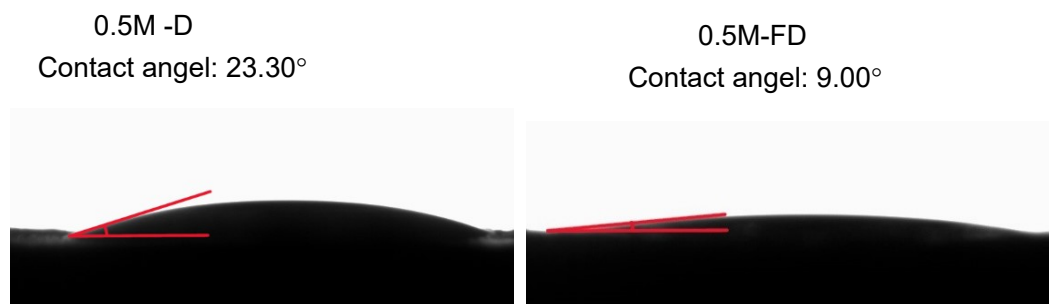


Fig. S4 Wettability test of the 0.5M-D and 0.5M-FD electrolytes on Celgard 2325 polyethylene separator.

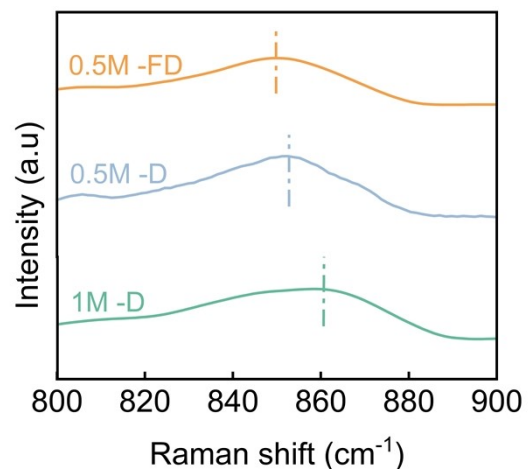


Fig. S5 Enlarged Raman spectra of three electrolytes in the range from 800 to 900 cm⁻¹.

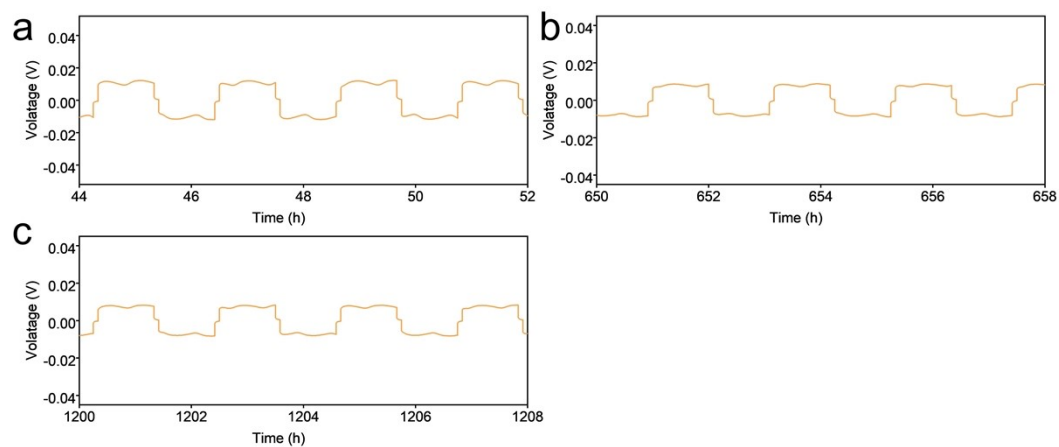


Fig. S6 The zoomed voltage-time profiles in the range of (a) 44–52 h, (b) 650–658 h and (c) 1200-1208 h.

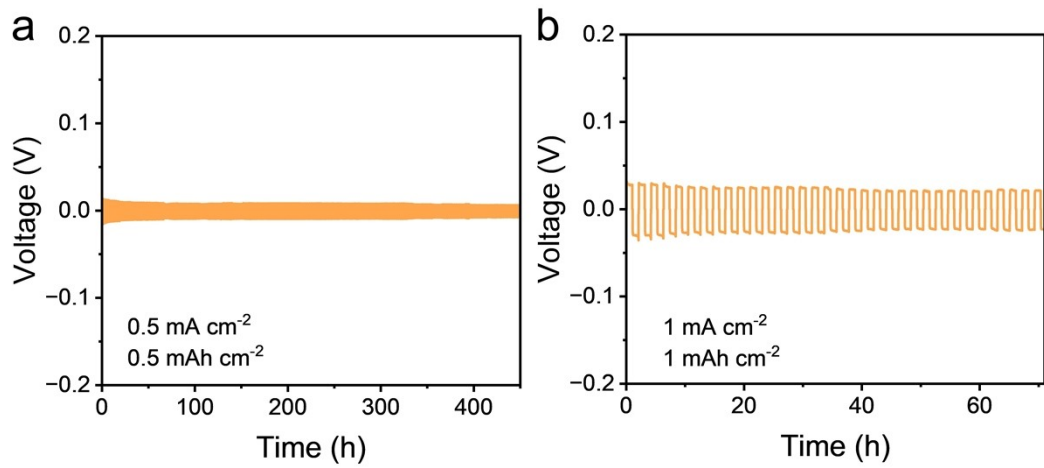


Fig. S7 Cycling performance of Na||Na cells with 0.5M-FD electrolyte at 0.5 mA cm^{-2} and 1 mA cm^{-2} under $-20 \text{ }^\circ\text{C}$.

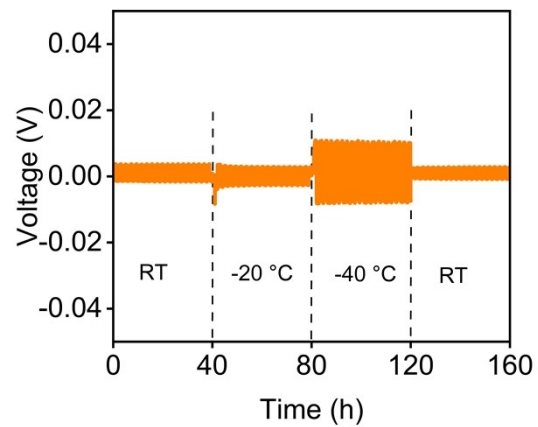


Fig. S8 The cycling performance of the Na||Na cell with the 0.5M-FD electrolyte at RT, -20 °C, -40 °C.

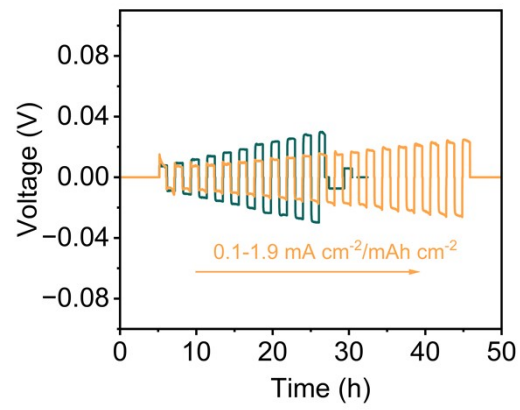


Fig. S9 The critical current density (CCD) measurements of Na||Na cells with 0.5M-D and 0.5M-FD electrolytes at different current densities ranging from 0.1 to 1.9 mA cm⁻² at -20 °C.

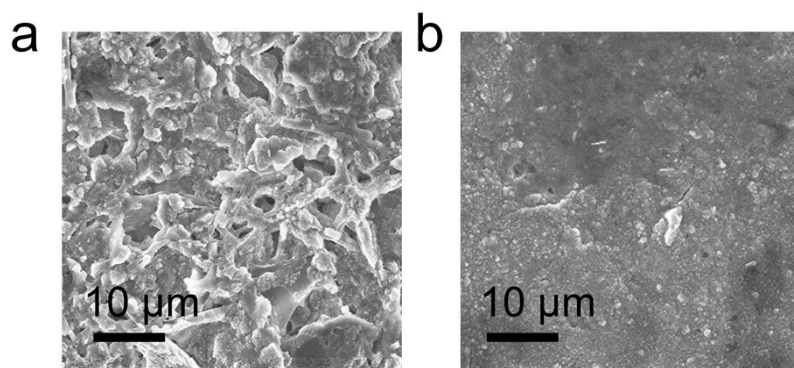


Fig. S10 SEM images of the deposited Na metal on Al/C current collectors in (a) 0.5M-D and (b) 0.5 M-FD electrolytes after 50 cycles of Na plating/stripping at 0.5 mA cm^{-2} and 0.5 mAh cm^{-2} under $-20 \text{ }^\circ\text{C}$.

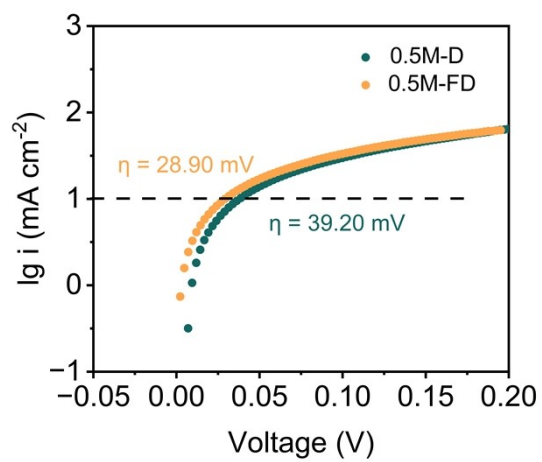


Fig. S11 Tafel plots of two investigated electrolytes in a three-electrode cell configuration.

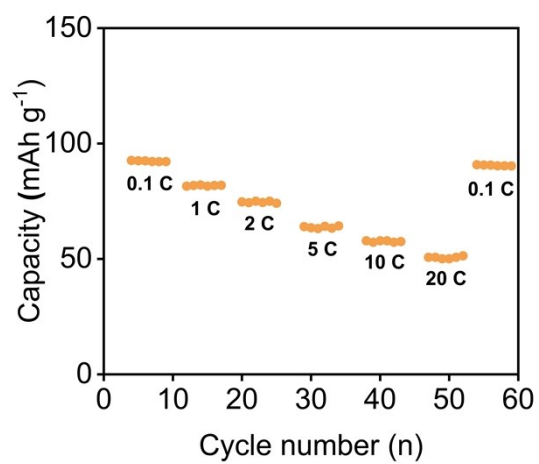


Fig. S12 Rate performance of Na||NVP cells with 0.5M-FD electrolyte at -20 °C.

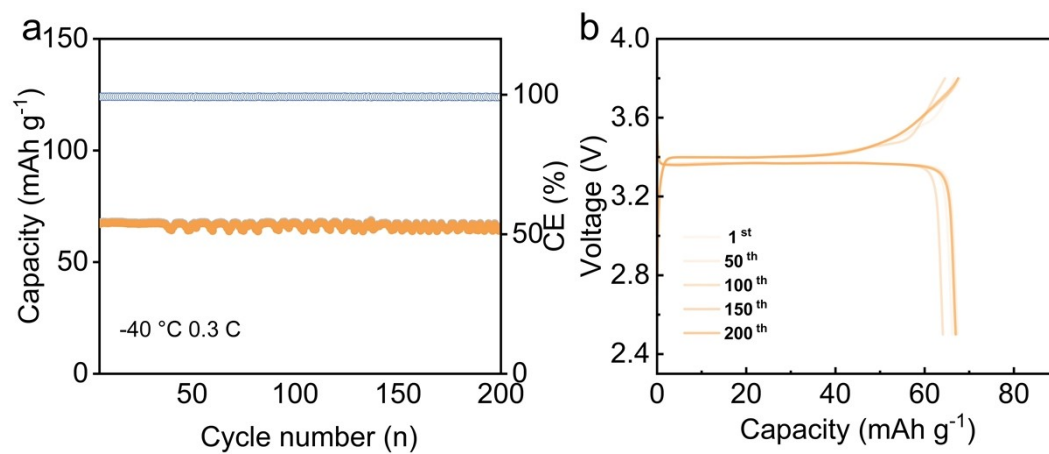


Fig. S13 (a) The cycling performance and (b) the representative voltage curves of the Na||NVP cell with 0.5M-FD electrolyte at 0.3 C and -40 °C.

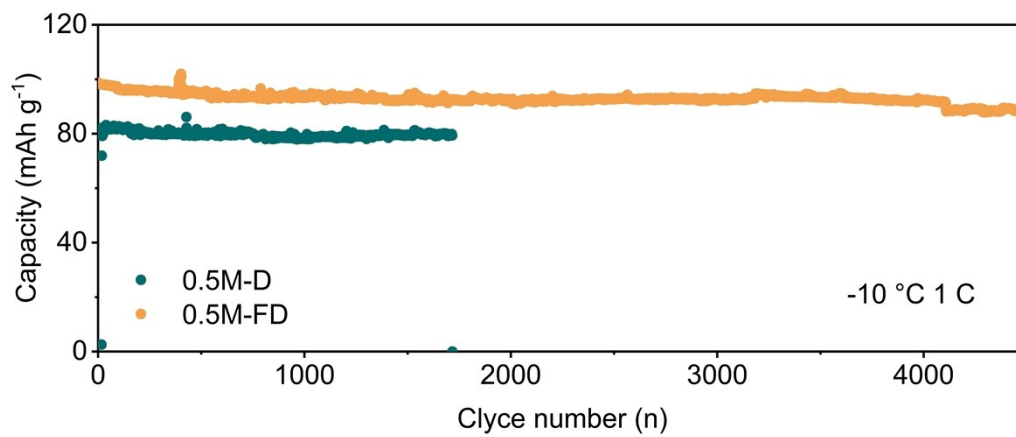


Fig. S14 The cycling performance of the Na||NVP cells with 0.5M-FD and 0.5M-D electrolyte at 1 C and -10 °C.

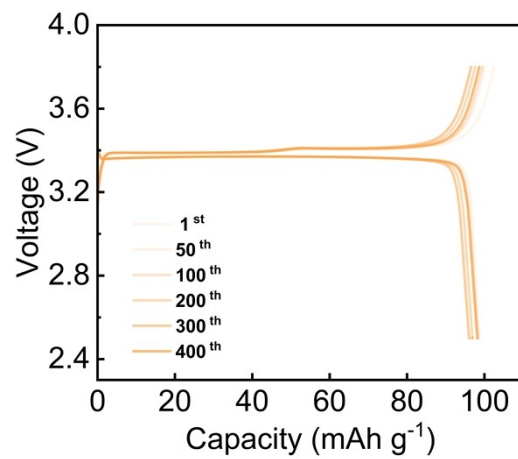


Fig. S15 The representative voltage curves of the Na || NVP cell with 0.5M-FD electrolyte at 1 C and -10 °C.

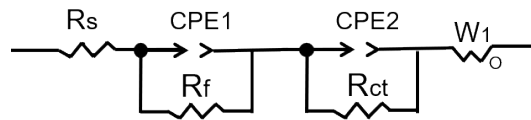


Fig. S16 The equivalent circuit for EIS fitting.

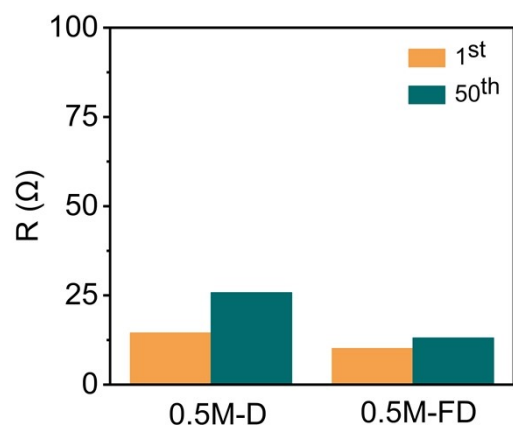


Fig. S17 The R values after 1 and 50 cycles for the 0.5M-D and 0.5M-FD electrolytes.

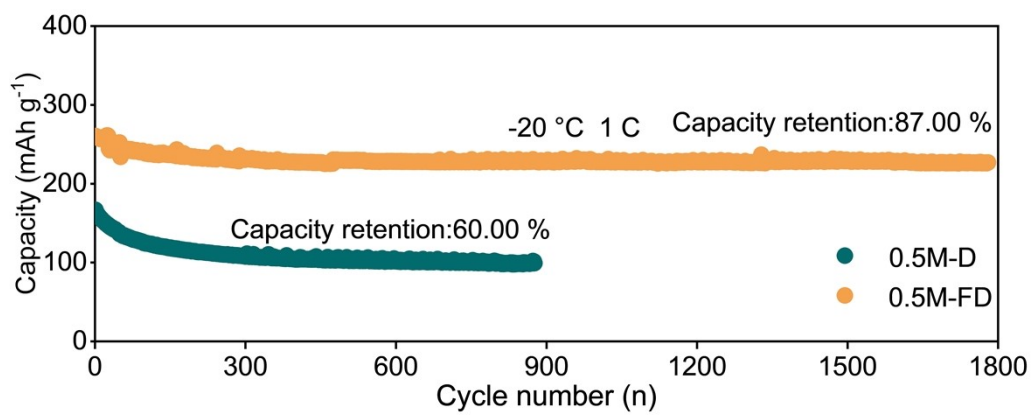


Fig. S18 The cycling performance of the Na||HC cells with 0.5M-FD and 0.5M-D electrolytes at 1 C and -20 °C.

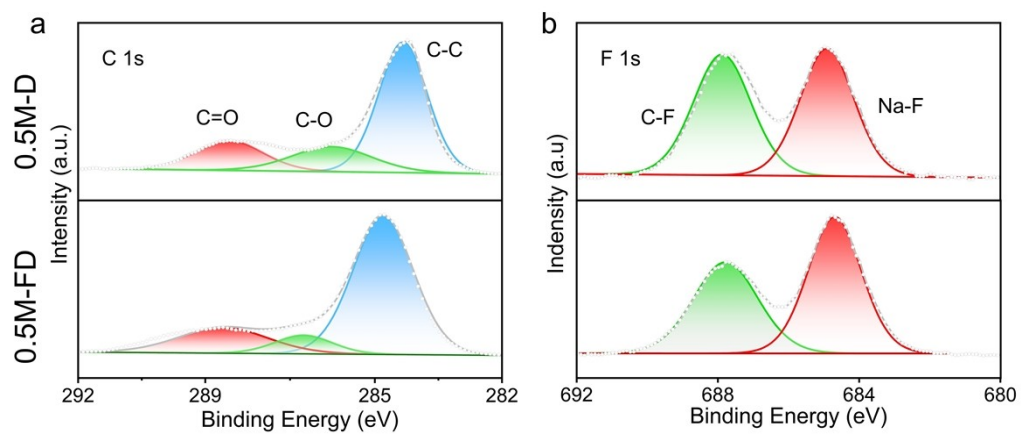


Fig. S19 XPS spectra of C1s (a) and F 1s (b) spectra of CEI on the surface of NVP cathode in the 0.5M-D and 0.5M-FD electrolytes.

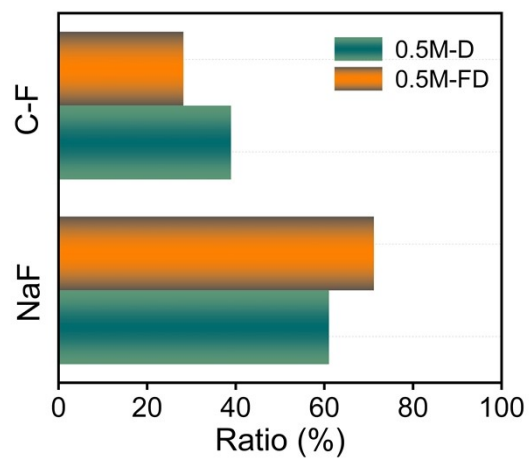


Fig. S20 The ratios of each component of CEI in the narrow spectra of F 1s.

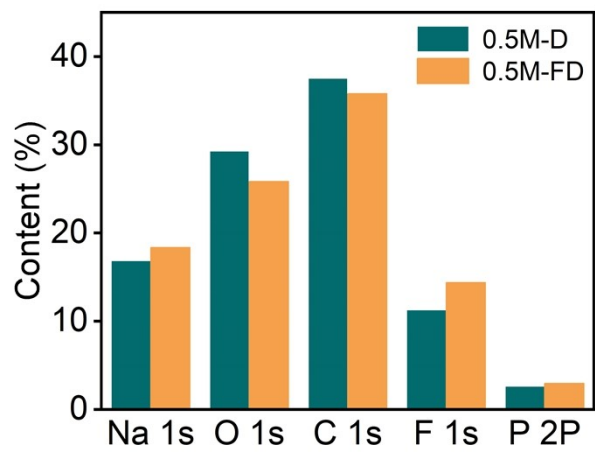


Fig. S21 Comparison of the element contents of CEI in the 0.5M-D electrolyte and 0.5M-FD electrolyte.

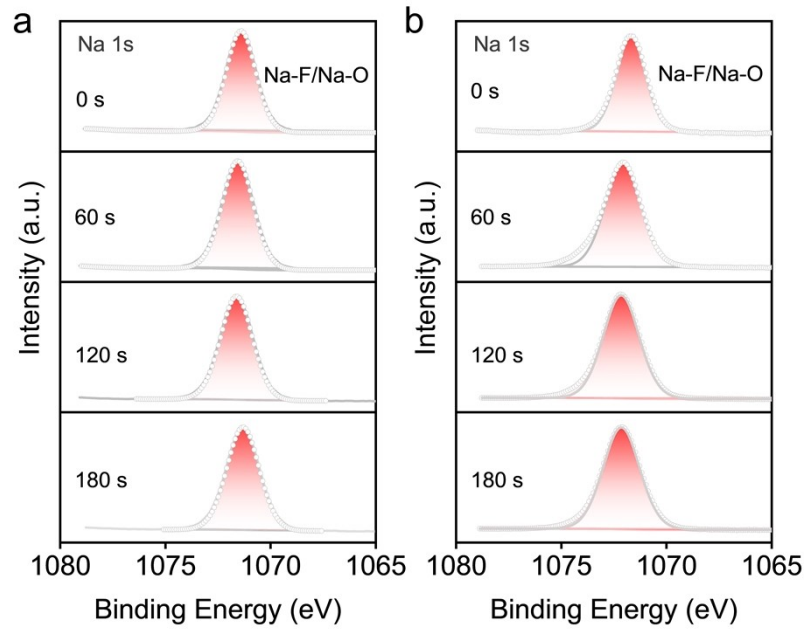


Fig. S22 The High-resolution XPS spectra of Na 1s spectra in the (a) 0.5M-D electrolyte and (b) 0.5M-FD electrolyte at the sputtering times of 0, 60 s, 120 s and 180 s.

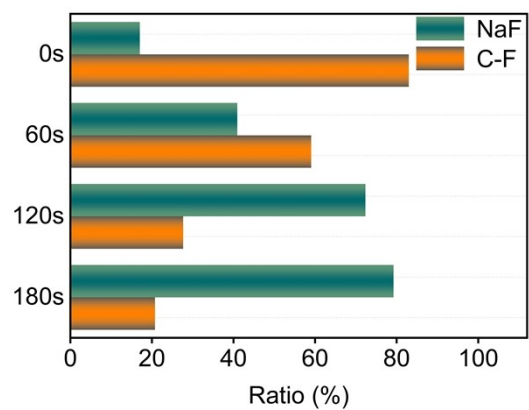


Fig. S23 The ratios of each component of SEI in the narrow spectra of F 1s with the 0.5M-FD electrolyte.

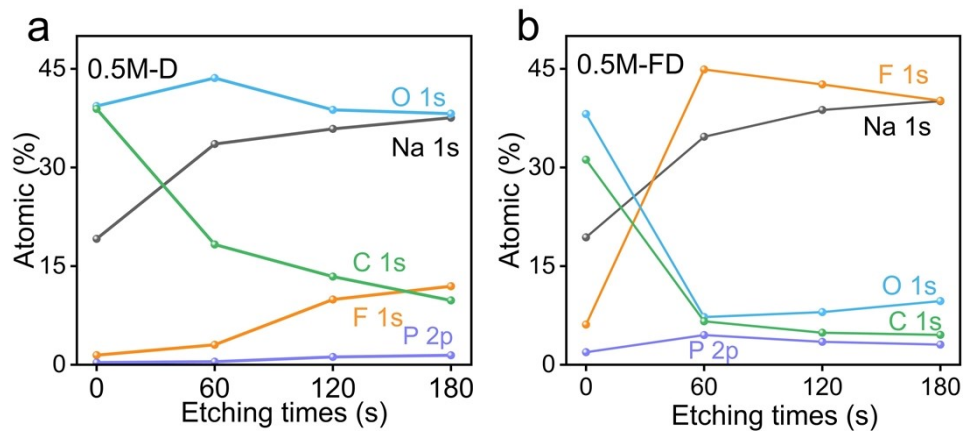


Fig. S24 Comparison of the element contents of SEI in (a) the 0.5M-D electrolyte and (b) 0.5M-FD electrolyte.

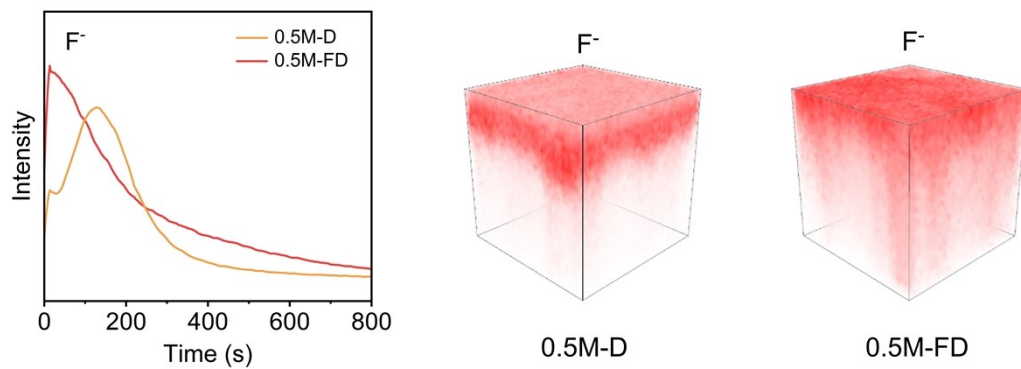


Fig. S25 3D rendering for the F^- secondary ions and the overlay in the TOF-SIMS tested for the SEI formed in the 0.5M-D and 0.5M-FD electrolyte.

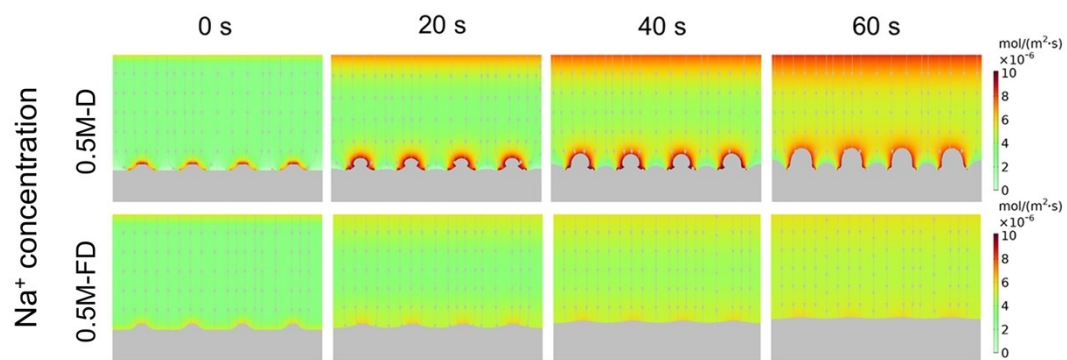


Fig. S26 COMSOL Multiphysics stimulation of Na⁺ concentration with 0.5M-D electrolyte and 0.5M-FD electrolyte.

Electrolyte formula	Capacity (mAh cm ⁻²)	Times (h)	Polarization voltage (V)	Refs.
1M NaFSI - EC/PC/DEC (1:1:4 by vol%) + 6 vol % ES	0.1	1500	≈ 1	s6
1 M NaPF ₆ -EC/DEC (1:1 by vol%) +1 wt.% ABAPE	0.5	200	≈ 1.5	s7
0.5 M NaOTf-DEGDME	1	500	0.05	s8
0.8 M NaOTf-THF/DME (1:3 by vol%)	1	580	≈ 0.1	s9
0.25 M NaOTf- 0.25 M NaPF ₆ -G2/TTE	0.5	560	0.022	s10
0.5M NaPF ₆ -DG+0.2 wt.%FPPN	0.1	1400	0.01	This work

References:

- [s1] W. Ma, X. Cui, Y. Chen, S. Wan, S. Zhao, J. Gong, G. Wang and S. Chen, *Angew Chem. Int. Ed.* 2024, **64**, e202415617.
- [s2] H. Sun, Z. Jin, C. Yang, R. L. C. Akkermans, S. H. Robertson, N. A. Spenley, S. Miller and S. M. Todd, *J. Mol. Model.* 2016, **22**, 47.
- [s3] S. Zhong, Y. Yu, Y. Yang, Y. Yao, L. Wang, S. He, Y. Yang, L. Liu, W. Sun, Y. Feng, H. Pan, X. Rui and Y. Yu, *Angew. Chem.* 2023, **135**, e202301169.
- [s4] X. Luo, M. Zhou, Z. Luo, T. Shi, L. Li, X. Xie, Y. Sun, X. Cao, M. Long, S. Liang and G. Fang, *Energy Storage Mater.* 2023, **57**, 628.
- [s5] Y.-L. Wang, F. U. Shah, S. Glavatskih, O. N. Antzutkin and A. Laaksonen, *J. Phys. Chem. B* 2014, **118**, 8711.
- [s6] S. E. Zhong, Y. S. Yu, Y. Yang, Y. Yao, L. F. Wang, S. N. He, Y. X. Yang, L. Liu, W. P. Sun, Y. Z. Feng, H. G. Pan, X. H. Rui and Y. Yu, *Angew Chem. Int. Ed.* 2023, **62**, e202301169.
- [s7] M. Li, J. L. Jiang, Y. Chen, S. S. Huang, X. Y. Liu, J. Yi, Y. Jiang, B. Zhao, W. R. Li, X. L. Sun and J. J. Zhang, *Angew. Chem. Int. Ed.* 2025, **64**, e202413806.
- [s8] C. Wang, A. C. Thenuwara, J. Luo, P. P. Shetty, M. T. McDowell, H. Zhu, S. Posada-Perez, H. Xiong and G. Hautier, W. Li, *Nat. Commun.* 2022, **13**, 4934.
- [s9] J. Zhou, Y. Wang, J. Wang, Y. Liu, Y. Li, L. Cheng, Y. Ding, S. Dong, Q. Zhu, M. Tang, Y. Wang, Y. Bi, R. Sun, Z. Wang and H. Wang, *Energy Storage Mater.* 2022, **50**, 47-54.
- [s10] D. Yu, Z. Wang, J. Yang, Y. Wang, Y. Li, Q. Zhu, X. Tu, D. Chen, J. Liang, U. Khalilov and H. Wang, *Small* 2024, **20**, 2311810.